Use of Lyapunov Exponents to Predict Chaotic Vessel Motions

Leigh McCue Armin Troesch

Department of Naval Architecture and Marine Engineering, University of Michigan

Abstract

It is the aim of this paper to further the use of Lyapunov and local Lyapunov exponent methods for analyzing phenomena involving nonlinear vessel dynamics. Lyapunov exponents represent a means to measure the rate of convergence or divergence of nearby trajectories thus denoting chaos and possibly leading to the onset of conditions that produce capsize. The work developed here makes use of Lyapunov exponent methodologies to study capsize and chaotic behavior in vessels both experimentally and numerically using a multi-degree of freedom computational model. Since, the Lyapunov exponent is defined in the limit as time approaches infinity, one encounters fundamental difficulties using Lyapunov exponents on the capsize problem, which is inherently limited to a finite time. This work also incorporates the use of local Lyapunov exponents, which do not require an infinite time series, to demonstrate their usefulness in analyzing finite time chaotic vessel phenomena. The objective is to demonstrate the value of the Lyapunov exponent and local Lyapunov exponent as a predictive tool with which to indicate regions with crucial sensitivity to initial conditions. Through the intelligent use of Lyapunov exponents in vessel analysis to indicate specific regions of questionable stability, one may significantly reduce the volume of costly simulation and experimentation.

Keywords: capsize, chaos, Lyapunov exponent, local Lyapunov exponent, nonlinear vessel motions

1 Background

The method of Lyapunov characteristic exponents serves as a useful tool to quantify chaos. Specifically, Lyapunov exponents measure the rates of convergence or divergence of nearby trajectories.(Haken, 1981; Wolf, 1986) Negative Lyapunov exponents indicate convergence, while positive Lyapunov exponents demonstrate divergence and chaos. The magnitude of the Lyapunov exponent is an indicator of the time scale on which chaotic behavior can be predicted or transients decay for the positive and negative exponent cases respectively (Wolf, 1986).

Physically, the Lyapunov exponent is a measure of how rapidly nearby trajectories converge or diverge. If one considers a ball of points in N-dimensional phase space, in which each point follows its own trajectory

based upon the system's equations of motion, over time, the ball of points will collapse to a single point, will stay a ball, or will become ellipsoid in shape (Glass & Mackey, 1988). The measure of the rate at which this infinitesimal ball collapses or expands is the Lyapunov exponent. For a system of equations written in state-space form $\dot{\mathbf{x}} = \mathbf{u}(x)$, small deviations from the trajectory can be expressed by the equation $\delta\dot{x}_i = (\partial u_i/\partial x_j)\delta x_j$ (Eckhardt & Yao, 1993). The maximal Lyapunov exponent is then defined by Equation 1.[1] Often times only the maximal Lyaponov exponent is discussed since the maximal exponent is simplest to calculate from a numerical time series and yields the greatest insight into the dynamics of the system. However, for a space with dimension N, there are N Lyapunov exponents which make up the Lyapunov spectrum and correspond to the rate of expansion or contraction of the principal axes of the infinitesimal N-dimensional ball. For example, after ordering Lyapunov exponents with λ_1 being the largest and λ_N being the smallest, the length of the most rapidly growing principal axis is proportional to $e^{\lambda_1 t}$, the area of the two most rapidly growing principal axes is proportional to $e^{(\lambda_1+\lambda_2)t}$, *etc...* (Wolf *et al.*, 1985). Other useful quantities are the short time Lyapunov exponent and the local Lyapunov exponent. A short time Lyapunov exponent is simply a Lyapunov exponent defined over some finite time interval. The local Lyapunov exponent is a short time Lyapunov exponent in the limit where the time interval approaches zero. Both are dependent on starting points, and the short time Lyapunov exponent is also dependent on the magnitude of the time interval. Equations for short and local Lyapunov exponents are presented in Equations 2 and 3 respectively (Eckhardt & Yao, 1993). Since it is not practically possible in a numeric or experimental sense to take the limit $T \to 0$, for the purposes of this paper the phrases 'short time' and 'local' Lyapunov exponents will be used interchangeably in reference to the approach given by Equation 2. Experimental data was collected with a time step of 0.033 s and thus for consistency the short time Lyapunov exponent is calculated at this interval in the numerical model.

$$\lambda_\infty = \lim_{t\to\infty} \frac{1}{t} \log \frac{\|\delta\mathbf{x}(t)\|}{\|\delta\mathbf{x}(0)\|} \tag{1}$$

$$\lambda_T(\mathbf{x}(t), \delta\mathbf{x}(0)) = \frac{1}{T} \log \frac{\|\delta\mathbf{x}(t+T)\|}{\|\delta\mathbf{x}(t)\|} \tag{2}$$

$$\lambda_{local}(\mathbf{x}(t)) = \lim_{T\to 0} \frac{1}{T} \log \frac{\|\delta\mathbf{x}(t+T)\|}{\|\delta\mathbf{x}(t)\|} \tag{3}$$

One can draw conclusions about the nature of the dynamical system from the spectra assembled. For a one-dimensional system a positive Lyapunov exponent indicates chaos, a negative exponent defines a periodic orbit, and a zero value represents an orbit with marginal stability.(Wolf *et al.*, 1985) For the case of a three-dimensional system there are three Lyapunov exponents making up the spectra. A fixed point consists of all negative exponents. A limit cycle's spectrum would have two negative values and a zero. A two-torus has two zeros and a negative value in it's spectrum, and a strange attractor has one each of positive, negative, and zero values.(Wolf *et al.*, 1985) This pattern can be extended to higher dimensional spaces.

[1]The Lyapunov exponent is defined with the logarithm base e. Depending on the nature of the application, at times the exponent is calculated base 2 in order to allow the output to be expressed in terms of bits per second. This lends physical insight as to a rate at which information about the state of the system is created or destroyed (Schuster, 1984). For consistency, in this work, the exponent is always calculated using the true definition base e and is therefore expressed with units of 1/time.

Since the Lyapunov spectrum is derived from a long-time evolution of an infinitesimal sphere, it is not a local quantity either spatially or temporally (Wolf *et al.*, 1985). Therefore, one of the potential benefits to examining the capsize problem through the method described by Lyapunov exponents, is the number of numerical or physical experiments necessary to draw quantitative conclusions can be drastically reduced from the quantity which would be necessary by brute force simulation.

This method has been touched on in previous naval architecture applications. Falzarano first noted without application the potential for using this to quantify chaotic ship dynamics (Falzarano, 1990). Papoulias (Papoulias, 1987) used Lyapunov characteristic exponent spectra to demonstrate the onset of chaotic behavior for a simulated tanker mooring system. Papoulias' model consisted of three degrees of freedom in surge, sway, and yaw and thus six state variables. He employed Lyapunov exponents to confirm instabilities for which he was already aware. The purpose of the following section, conversely, is to demonstrate that Lyapunov exponents can be used to indicate regions of instability for which further analysis is required. Additionally, Murashige and Aihara make reference the use of Lyapunov exponents in analyzing capsizing models for a flooded ship in regular beam seas (Murashige & Aihara, 1998). While their model accounts for some of the complexities associated with a flooded ship, it neglects sway and heave motion (Murashige & Aihara, 1998). Additionally, their analysis of Lyapunov exponents is limited to their numerical model. They do not validate their Lyapunov prediction with their experimental result, and their Lyapunov calculation is limited to one marginally unstable case in which capsize does not occur. Arnold *et al* conducted a thorough numerical study of the single degree of freedom capsize case, but their work is limited to a one degree of freedom numerical model using solely the long time Lyapunov exponent (Arnold *et al.*, 2003).

The work of the following sections provides a more complete investigation into the use of Lyapunov exponents for analyzing stable, marginally unstable, and unstable dynamics leading to capsize. The goal is to evaluate Lyapunov exponents as a predictive tool with which to indicate regions of crucial sensitivity to initial conditions. To allow for detailed investigation into regions of questionable stability, one may reduce the necessary volume of simulations and experimentation of the entire phase space through intelligent use of Lyapunov exponents. Additionally, since the Lyapunov exponent provides a quantitative value, it can be used as a tool to directly compare the accuracy of a numerical model to experimental runs. Rather than attempting to qualitatively evaluate a numerical tool through predicting capsize with a heads or tails type comparison of capsize versus non-capsize, the Lyapunov exponent can be used to demonstrate that a numerical model is in fact simulating the same type, or magnitude of chaos as experiments.

2 Lyapunov exponents from experimental time series

2.1 Theory

A large volume of work has been dedicated to the problem of calculating Lyapunov exponents from experimental time series. A number of researchers have developed methods which can be divided into two distinct approaches, direct methods and tangent space methods.

Direct methods consist of searching the time series for neighbors at any given point and calculating expansion rates through comparison to these neighboring points. The first such method was that of Wolf *et al* (1985). Wolf *et al* (1985) developed a methodology in which one can calculate the largest positive Lyapunov exponent from a data set by following the long term evolution of one principal axis, a 'fiducial trajectory', progressively reorthonormalized maintaining phase space orientation (Wolf *et al.*, 1985). Wolf's method is highly sensitive to inputs, however, and can easily lead to an erroneous result. In the early 1990's two separate research groups produced a new method (Rosenstein *et al.*, 1993; Kantz, 1994). The approach eliminates the requirement Wolf imposes upon maintaining phase-space orientation stating it is unnecessary for calculating the largest Lyapunov exponent (Rosenstein *et al.*, 1993). Additionally, rather than following one trajectory, the full data set is used, and in essence a trajectory for every pair of nearest neighbors is calculated. For details refer to Rosenstein *et al* (1993) and Kantz (1994). Both methods are substantively similar. The Kantz algorithm (and similarly the Rosenstein algorithm) calculates the largest Lyapunov exponent by searching for all neighbors within a neighborhood of the reference trajectory and computes the average distance between neighbors and the reference trajectory as a function of time (or relative time scaled by the sampling rate of the data) (Kantz, 1994; Rosenstein *et al.*, 1993). The algorithm computes values for Equation 4 with parameters defined as follows: x_t, arbitrary point in time series; U_t, neighborhood of x_t; x_i neighbor of x_t; τ, relative time scaled by sampling rate; T length of time series; $S(\tau)$ stretching factor with region of robust linear increase showing slope equal to Lyapunov exponent *ie* $e^{\lambda\tau} \propto e^{S(\tau)}$ (Kantz, 1994; Kantz & Schreiber, 2004). However, this post-processing requirement of a robust linear increase in slope introduces new errors. While the method is useful and accurate for systems with known values for the Lyapunov exponent, the choice of region and parameters over which a 'robust linear increase' are found is somewhat arbitrary. It is the opinion of the authors that this tool is useful only if one knows what value of Lyapunov exponent is desired and can thus choose the region exhibiting a slope equal to that value.

$$S(\tau) = \frac{1}{T}\sum_{t=1}^{T} \ln\left(\frac{1}{|U_t|}\sum_{i\epsilon U_t} |x_{t+\tau} - x_{i+\tau}|\right) \tag{4}$$

Tangent space methods, developed simultaneously by the separate research teams of Sano and Sawada (1985) and Eckmann and coauthors (1985; 1986) allow for calculation of the full spectrum of Lyapunov exponents through local predictions of the Jacobian along the time series trajectory. For example, for a given trajectory $\mathbf{x}$(t) defined by Equation 5, the tangent vector ξ is given by the linearized form of Equation 5 presented in Equation 6 where $\mathbf{J}$ is the Jacobian matrix of $\mathbf{f}$, $\mathbf{J} = \partial\mathbf{f}/\partial\mathbf{x}$ (Sano & Sawada, 1985). Sano and Sawada (1985) solve Equation 6 through a least squares estimate of the time dependent linear operator A_j which approximates the map from $\xi(0)$ to $\xi(t)$. The Lyapunov exponents are then computed using Equation 7 where τ is a flow scale time increment, n is then number of data points, and $\mathbf{e}$ is an orthonormal basis maintained using a Gram-Schmidt renormalization process (Sano & Sawada, 1985). For details of this process refer to Sano and Sawada (1985) or the similar works of Eckmann *et al* (1985; 1986).

$$\dot{\mathbf{x}} = \mathbf{f}(\mathbf{x}) \tag{5}$$

$$\dot{\xi} = \mathbf{J}(\mathbf{x}(t)) \cdot \xi \tag{6}$$

$$\lambda_i \quad = \quad \lim_{n\to\infty} \frac{1}{n\tau} \sum_{j=1}^{n} \ln \|A_j \mathbf{e}_i^j\| \tag{7}$$

The weakness of this approach is in its sensitivity to choice of embedding dimension. Too small an embedding dimension outputs erroneous Lyapunov exponents while too large an embedding dimension creates spurious exponents (Kantz, 1994). However, for this application with careful attention paid to the choice of embedding dimension, the tangent space method was found to be more robust then the direct methods as it was not dependent on any form of arbitrary postprocessing. To check for spurious exponents, the technique first suggested by Parlitz (1992) of analyzing both the original time series and the reversal of the original time series was used. No significant errors were noted for the largest Lyapunov exponents presented in this work. The implementation of the Sano and Sawada method included in the TISEAN (Hegger *et al.*, 2000) package was used to calculate Lyapunov exponents for the experimental time series in the following subsections.

2.2 Application to the capsize problem

The Sano and Sawada algorithm (1985) contained in TISEAN (Hegger *et al.*, 2000) was applied to roll time series for the capsize and non-capsize experiments detailed in works by Obar and Lee (2001) and Lee *et al* (2004) with an embedding dimension equal to 6 to represent the six state-space variables. The physical model used in the experimental analysis and replicated numerically was a box barge featuring the following principal parameters: beam, $B = 30.48$ cm; beam/draft, $B/T = 1.67$; depth/draft, $D/T = 1.06$; beam/wave length, $B/\lambda = 0.23$; wave amplitude/wave length, $\zeta_o/\lambda = 0.01$; roll natural frequency $\omega_n = 2.28$ rad/s; excitation frequency/roll natural frequency, $\omega_e/\omega_n = 3.0$; and angle of vanishing stability $\theta_v = 11.4$ degrees. The results of completing the process of using Sano and Sawada's algorithm to calculate the largest Lyapunov exponent for all capsize and non-capsize runs are presented in Figure 1. As one might expect, there is relatively little variation in Lyapunov exponent values. The mean Lyapunov exponent for all runs is 1.76 s^{-1}. The mean exponent for capsize runs, 1.83 s^{-1} is somewhat larger than that of non-capsize runs, 1.57 s^{-1} with significantly larger outliers. The histograms in Figure 2 show the distribution of Lyapunov exponents for both the capsize and non-capsize cases. Due to the brevity of the time series leading to capsize, it is impossible to confirm convergence of the Lyapunov exponent. However, it is feasible to discern an order of magnitude of the Lyapunov exponent with which to compare the numerical model as well as to conclude that runs leading to capsize are more chaotic in nature than those not leading to capsize as is apparent in Figures 1-2. The Lyapunov exponent is, by definition, an infinite time parameter, but by nature capsize is a finite event. For this reason greater insight can be gleaned through calculation of the local Lyapunov exponent as will be discussed in Section 4. It should be noted that all runs result in a positive, chaotic, Lyapunov exponent. Recall that under the definition of the Lyapunov exponent a stable limit cycle would have a zero Lyapunov exponent. Therefore, the motions measured in the six dimensional state-space are growing rather that oscillating sinusoidally. Chaotic behavior is detected even in the non-capsize case.

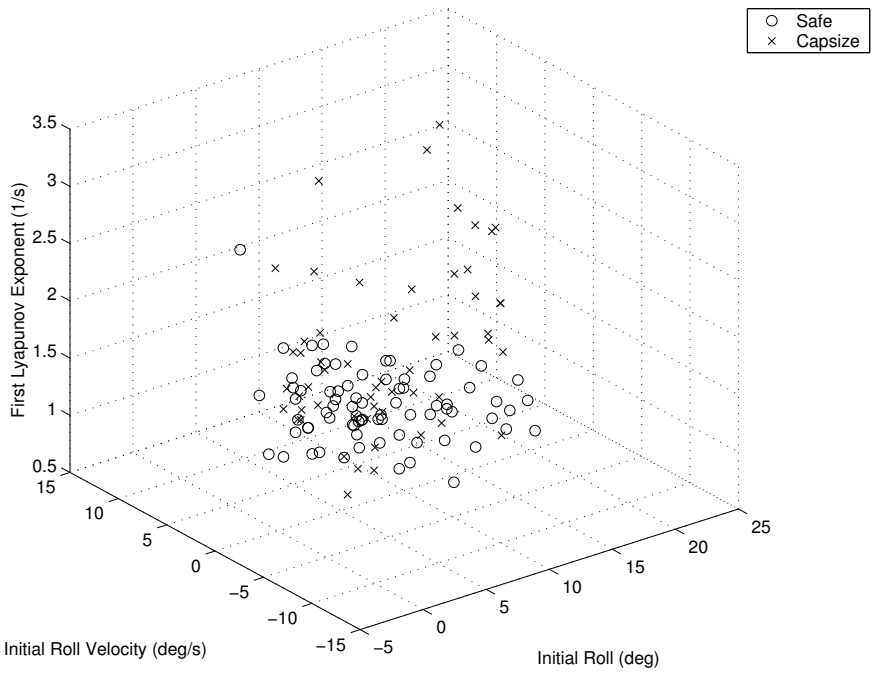

Figure 1: Lyapunov exponents based on experimental time series. Phase space showing Lyapunov exponents versus roll and roll velocity initial conditions sampled at time t_o. Model release time and length of time series variable between runs.

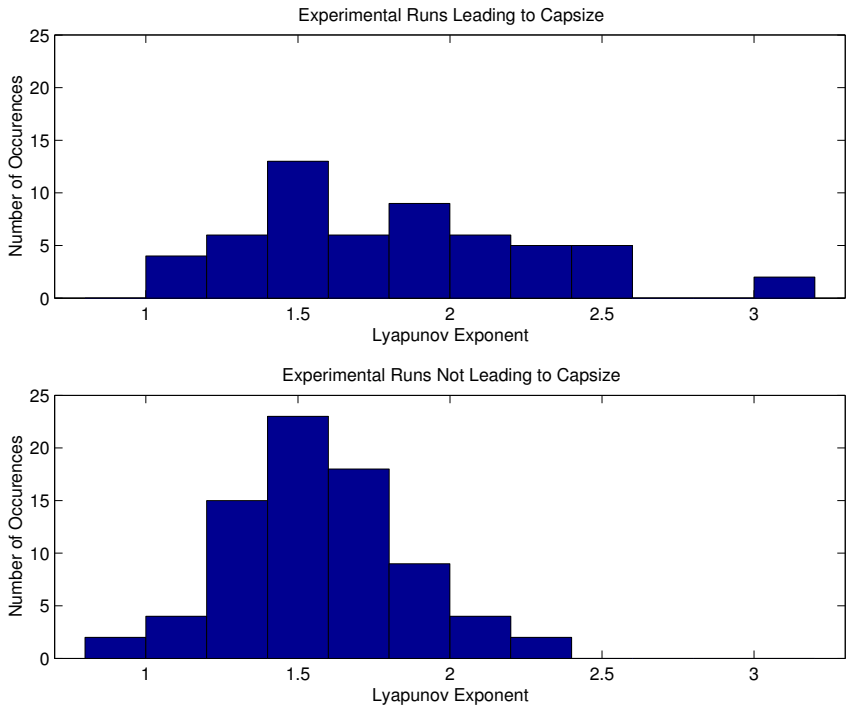

Figure 2: Histograms of Lyapunov exponent values for runs leading to capsize and non-capsize.

3 Lyapunov exponents from ordinary differential equations

3.1 Theory

As discussed in the previous section, the Lyapunov exponents measure the evolution of an infinitesimal sphere. However, infinitesimal quantities are not computationally feasible, and for a chaotic system with a finite initial separation between the principal axes of the sphere, it is impossible to assure convergence of solution for Lyapunov exponents before infinite values are encountered (Wolf, 1986; Wolf *et al.*, 1985). Therefore, other means of evaluation are necessary.

To overcome this difficulty, Benettin *et al* proposed a method in which the trajectory of the center of the infinitesimal sphere, the fiducial trajectory, is defined by the nonlinear equations based upon initial conditions.(Benettin *et al.*, 1980) Principal axes are then calculated from the linearized form of the equations of motion about the fiducial trajectory (Wolf, 1986). These axes will, by definition, be infinitesimal relative to the attractor (Wolf *et al.*, 1985). In implementation two computational difficulties arise, namely, computational limitations prohibit calculation of exponential growth and all basis vectors will have a tendency towards the direction of most rapid growth allowing for calculation of only the largest Lyapunov exponent (Wolf *et al.*, 1985). To overcome these computational difficulties a Gram-Schmidt orthonormalization procedure is used (Wolf *et al.*, 1985; Bay, 1999). Through noting the magnitude of vectors prior to re-normalization, growth rates are calculated. Additionally, by maintaining an orthonormal basis all Lyapunov exponents can be calculated. The first vector will naturally tend towards the largest rate of growth, the second vector towards the second most rapid growth rate, and so on (Wolf *et al.*, 1985). Through the use of a Gram-Schmidt reorthonormalization the rapidly growing axes can be renormalized to represent an orthonormal basis maintaining the volume's phase-space orientation (Wolf, 1986; Wolf *et al.*, 1985). For further details on this process refer to (Benettin *et al.*, 1980; Lichtenberg & Lieberman, 1983; Parker & Chua, 1989; Seydel, 1988; Wolf, 1986; Wolf *et al.*, 1985).

3.2 Application to the capsize problem

3.2.1 Implementation

Calculating the Jacobian of the equations of motion used in the numerical simulator (Obar *et al.*, 2001; McCue & Troesch, 2003; Lee *et al.*, 2004), given by Equation 8 is non-trivial. While the mass and linear damping terms are easily treated, the quadratic damping and forcing terms require extra consideration.

$$\begin{bmatrix} m+a_{22} & 0 & a_{24} \\ 0 & m+a_{33} & 0 \\ a_{42} & 0 & I_{cg}+a_{44} \end{bmatrix} \begin{pmatrix} \ddot{x}_g \\ \ddot{y}_g \\ \ddot{\phi} \end{pmatrix} + \begin{bmatrix} b_{22} & 0 & b_{24} \\ 0 & b_{33} & 0 \\ b_{42} & 0 & b_1 \end{bmatrix} \begin{pmatrix} \dot{x}_g \\ \dot{y}_g \\ \dot{\phi} \end{pmatrix} \tag{8}$$

$$+ \begin{bmatrix} 0 & 0 & 0 \\ 0 & 0 & 0 \\ 0 & 0 & b_2 \end{bmatrix} \begin{pmatrix} 0 \\ 0 \\ \dot{\phi}|\dot{\phi}| \end{pmatrix} = \begin{pmatrix} \rho g_{e_2} \nabla + f_2^D \\ \rho g_{e_3} \nabla - mg + f_3^D \\ \rho g_{e4} GZ \nabla + f_4^D \end{pmatrix}$$

Two approaches to treat the quadratic damping term are as follows. One method is to replace, in the linearized model, the term $\dot{\phi}|\dot{\phi}|$ with $\dot{\phi}^2$ for $\dot{\phi} > 0$, $-\dot{\phi}^2$ for $\dot{\phi} < 0$, and assume that the precise singularity at $\dot{\phi} = 0$ will never be encountered due to double precision computational accuracy. The second approach is to use Dalzell's (1978) treatment for quadratic damping. Dalzell (1978) fits an odd function series of the form $\dot{\phi}|\dot{\phi}| = \sum_{k=1,3,\ldots} \alpha_k \frac{\dot{\phi}^k}{\dot{\phi}_c^{k-2}}$. Solving for α_k the truncated third order fit becomes $\dot{\phi}|\dot{\phi}| \approx \frac{5}{16}\dot{\phi}\dot{\phi}_c + \frac{35}{48}\frac{\dot{\phi}^3}{\dot{\phi}_c}$ over some range $-\dot{\phi}_c < \dot{\phi} < \dot{\phi}_c$ (Dalzell, 1978). Basic testing indicated both treatments yield similar results, therefore the Dalzell treatment, with $\dot{\phi}_c = 10$ degrees, was used for the results presented herein to avoid any difficulties due to the singularity associated with the first method.

The linearized influence of the forcing side of the equation is calculated using a simple differencing scheme. Forces are calculated as the difference between their values on the fiducial trajectory and their values at the offset from the trajectory. Due to linear superposition this can be calculated in a more computationally efficient manner for the differential at $(x + \delta x, y + \delta y, \phi + \delta\phi, t)$ rather than conducting the summation of force differentials at $(x + \delta x, y, \phi, t)$, $(x, y + \delta y, \phi, t)$, and $(x, y, \phi + \delta\phi, t)$. Therefore, the linearized form of the equations of motion about the fiducial trajectory are written as Equation 9:

$$\begin{bmatrix} m + a_{22} & 0 & a_{24} \\ 0 & m + a_{33} & 0 \\ a_{42} & 0 & I_{cg} + a_{44} \end{bmatrix} \begin{pmatrix} \delta\ddot{x}_g \\ \delta\ddot{y}_g \\ \delta\ddot{\phi} \end{pmatrix} + \begin{bmatrix} b_{22} & 0 & b_{24} \\ 0 & b_{33} & 0 \\ b_{42} & 0 & b_1 \end{bmatrix} \begin{pmatrix} \delta\dot{x}_g \\ \delta\dot{y}_g \\ \delta\dot{\phi} \end{pmatrix}$$
$$+ \begin{bmatrix} 0 & 0 & 0 \\ 0 & 0 & 0 \\ 0 & 0 & b_2(\frac{5}{16}\dot{\phi}_c + \frac{35}{16}\frac{\dot{\phi}^2}{\dot{\phi}_c}) \end{bmatrix} \begin{pmatrix} 0 \\ 0 \\ \delta\dot{\phi} \end{pmatrix} = \tag{9}$$
$$\begin{pmatrix} \rho g_{e_2}\nabla + f_2^D \\ \rho g_{e_3}\nabla - mg + f_3^D \\ \rho g_{e4} GZ\nabla + f_4^D \end{pmatrix}_{(x+\delta x, y+\delta y, \phi+\delta\phi, t)} - \begin{pmatrix} \rho g_{e_2}\nabla + f_2^D \\ \rho g_{e_3}\nabla - mg + f_3^D \\ \rho g_{e4} GZ\nabla + f_4^D \end{pmatrix}_{(x,y,\phi,t)}$$

Six sets of these linearized equations are integrated in time to calculate the ith Lyapunov exponent for i=1,6 by measuring the logarithm of the rates of growth of the six systems. Numerically this corresponds to the discrete representation of Equation 1 as Equation 10 in which 'm' represents the number of renormalization steps conducted and 'L' denotes the length of each element. The methodology employed is derived from that published by Wolf and coauthors (Wolf *et al.*, 1985; Wolf, 1986).

$$(\lambda_1)_m = \frac{1}{t}\sum_{j=1}^{m} \log \frac{L(t_{j+1})}{L(t_j)} \tag{10}$$

3.2.2 Results

Figure 3 presents a three-dimensional phase space portrayal with the value of the first Lyapunov exponent plotted on the z-axis. Ten minutes of simulated data was collected for non-capsize runs and capsize runs were simulated until the point of capsize. Initially this plot could appear enigmatic. Graphically, it is apparent that all non-capsize runs result in an equal valued positive Lyapunov exponent of approximately 1.77 s^{-1} after 600 simulated seconds. Intuitively it is expected that capsize runs would have larger Lyapunov

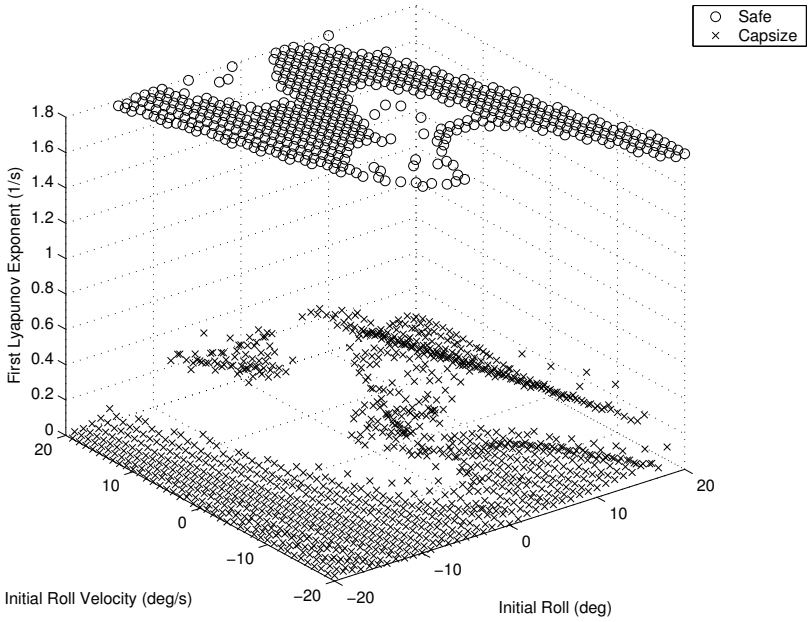

Figure 3: Lyapunov exponents based on numerical simulation. Phase space showing Lyapunov exponents versus roll and roll velocity initial conditions with numerical model released at t_o.

exponent values than non-capsize, however capsize runs all feature small, even near-zero Lyapunov exponents.

To make physical sense of this counter-intuitive result consider Figure 4 which shows the convergence, or lack thereof, of Lyapunov exponents for neighboring capsize and non-capsize cases. In Figure 4 it is evident that the time series resulting in capsize is too short to allow for convergence of the Lyapunov exponent. While the Lyapunov exponent of both the non-capsize and capsize cases follow closely, it is only immediately before capsize that the value of the Lyapunov exponent for the capsize case rises somewhat above the value of the Lyapunov exponent for the non-capsize case. Yet capsize occurs sufficiently rapidly as to prevent convergence of the exponent and instead results in small, non-converging, Lyapunov exponents. This explains the small values of Lyapunov exponents for capsize runs shown in Figure 3. As is evident, hundreds of cycles are necessary for exponent convergence.

Even with a lack of convergence of the Lyapunov exponent for capsize cases, key information can be derived from the result. Primarily, since the Lyapunov exponent is an indicator of the magnitude of the chaos of the system, by way of comparison of experimental and numerical results for large amplitude motions near capsize this methodology serves as a validation tool for the numerical model. Consider Figures 1 and 3. In Section 2 it was shown that the Lyapunov exponent for experimental runs not leading to capsize was 1.57 s^{-1}. This value is close to the Lyapunov exponent of approximately 1.77 s^{-1} for non-capsize runs using the numerical model. Additionally, due to the finite nature of the experimental tests, it is anticipated that if it were feasible to collect data over longer time interval, such as the ten minute interval over which the numerical model was simulated, the experimental Lyapunov exponent would converge to a somewhat larger value thus reducing the difference between the two mean exponents. It is impossible then to calculate

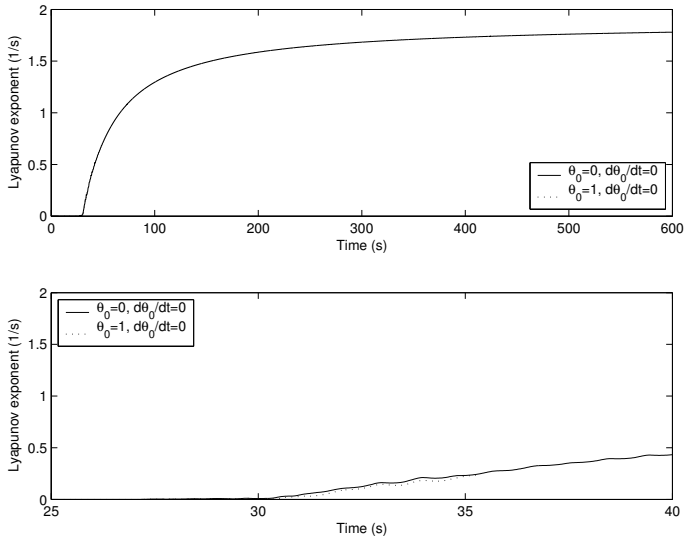

Figure 4: Numerically calculated Lyapunov exponent as a function of time for neighboring capsize and non-capsize cases. Top panel shows full time series from $t = 0$ to $t = 600$. Bottom panel shows identical data over critical region from $t = 25$ to $t = 40$. Both runs released with zero initial roll velocity, sway, sway velocity, heave, or heave velocity. Initial roll for non-capsize and capsize runs equal to 0 and 1 degree respectively.

an accurate value of the Lyapunov exponent for a capsize run. To understand the chaotic behavior leading to capsize it is important to consider a short term Lyapunov exponent instead as is discussed in Section 4.

4 Short time Lyapunov exponents from ordinary differential equations

4.1 Implementation

The short time Lyapunov exponent from ordinary differential equations is calculated in much the same manner as the Lyapunov exponent. Again, 'n' sets of differential equations linearized about the fiducial trajectory are calculated to measure incrementally stretching and shrinking principal axes. The 'n' linearized sets, where 'n' is the dimension of the phase space, are reorthonormalized after each step. Numerically, Equation 2 is calculated as Equation 11.

$$\lambda_1(\mathbf{x}(\mathbf{t}), \Delta t) = \frac{1}{\Delta t} \log \frac{L(t + \Delta t)}{L(t)} \tag{11}$$

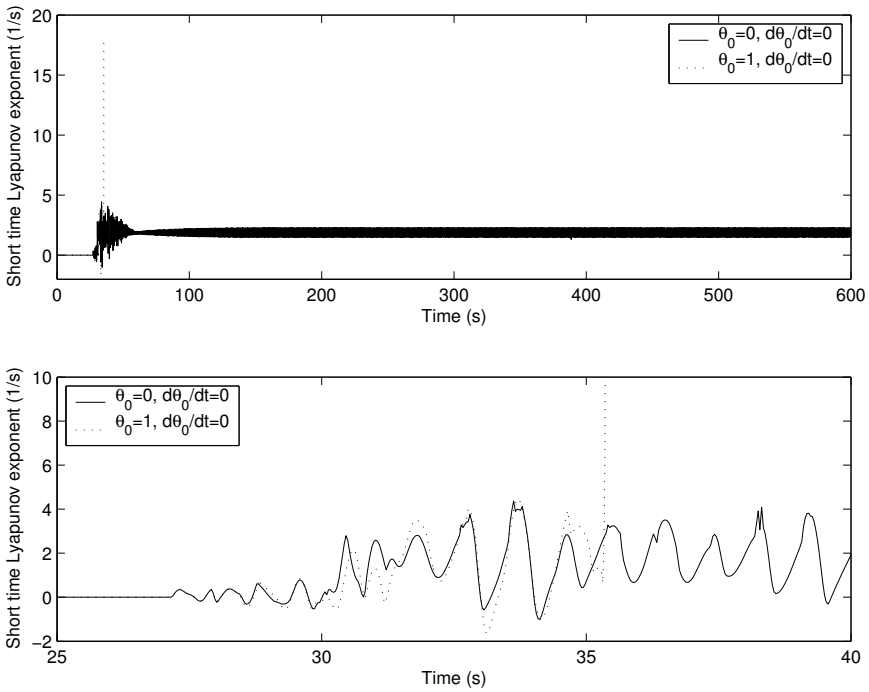

Figure 5: Numerically calculated short time Lyapunov exponent as a function of time for neighboring capsize and non-capsize cases. Top panel shows full time series from $t = 0$ to $t = 600$. Bottom panel shows identical data over critical region from $t = 25$ to $t = 40$. Both runs released with zero initial roll velocity, sway, sway velocity, heave, or heave velocity. Initial roll for non-capsize and capsize runs equal to 0 and 1 degree respectively.

4.2 Results

Consider Figure 5 in comparison to Figure 4. In both figures the numerical model is released at t_o, the location of the maximum transient wave peak, or 27.1705 seconds (Lee *et al.*, 2004). Figure 5 shows the short time Lyapunov exponent as a function of time for the same neighboring cases leading to capsize and non-capsize. The non-capsize case rises to a maximum value of 4.37 s^{-1} then, similarly to Figure 4, converges to oscillatory behavior about a short time Lyapunov exponent of 1.85 s^{-1}. However, for the capsize case useful predictive information is now visible. For the last few steps prior to capsize the short time Lyapunov exponent is larger than the short time Lyapunov exponent for non-capsize although they initially feature similar behavior. At capsize the short time Lyapunov exponent rapidly increases to a value an order of magnitude larger than that of the non-capsize case.

Figure 6 presents the values of short time Lyapunov exponent as a function of initial roll and roll velocities. While Figure 3 featured relatively invariant values of Lyapunov exponent based upon capsize or non-capsize, Figure 6 yields a range of short time Lyapunov exponents for runs leading to capsize. In Figure 6 runs not leading to capsize all feature peak short time Lyapunov exponent values near 4.2 s^{-1} as shown by the histogram plot of the same data given in Figure 7. However, as seen in Figure 7 runs leading to capsize have a wide range of values for short time Lyapunov exponent with a mean of 8.3 s^{-1} and a standard deviation

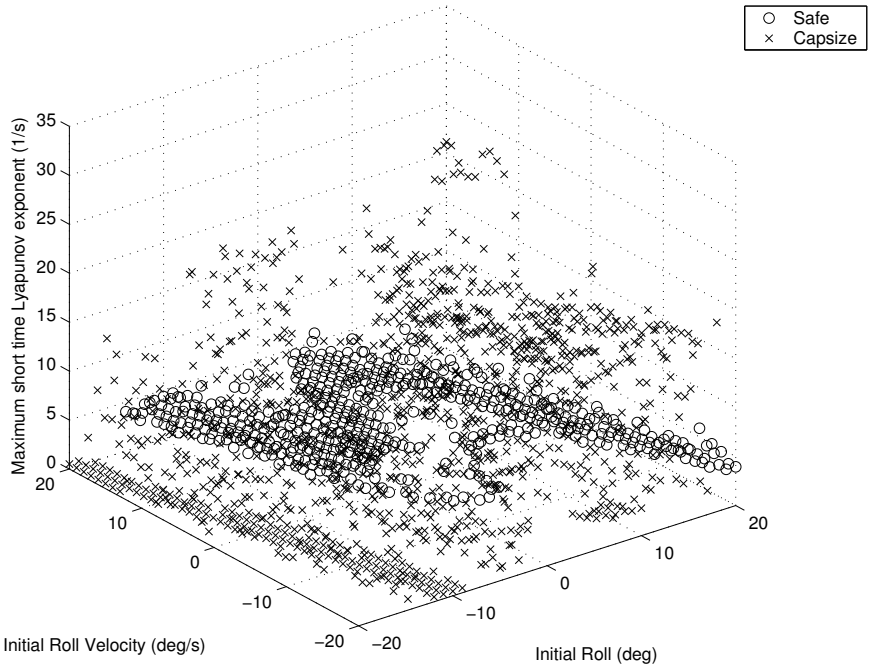

Figure 6: Short time Lyapunov exponents based on numerical simulation. Phase space showing short time Lyapunov exponents versus roll and roll velocity initial conditions with numerical model released at t_o.

of 6.1 s^{-1}, an order of magnitude larger than the standard deviation of the peak first short time Lyapunov exponent for runs not leading to capsize.

It should be noted that peak short time Lyapunov exponent for capsize runs ranges from near zero to 33 s^{-1}. It is the hypothesis of the authors that capsize runs featuring small short time Lyapunov exponents are a result of a 'blue sky catastrophe' or a process with hysteresis as discussed by Thompson and coauthors (1987) and Lee *et al* (2004). In such cases the rapid growth of the capsize attractor results in a capsize which is potentially difficult to detect unless the time interval of measurement is exceedingly small. This is consistent with the top panel of Figure 8 which indicates that the bulk of the runs with both the smallest and largest local Lyapunov exponents capsize within the first time steps immediately after the maximal exponent and the bottom panel which shows that the smallest Lyapunov exponents are found for runs which capsize within the first two cycles after release. Analysis of Figure 6 also indicates that that those capsize runs with smallest local Lyapunov exponent tend to be found at large negative initial roll angles. Many of these roll angles are statistically unlikely to occur and therefore choosing initial limits of phase space using a statistically validated methodology, such as that described in McCue and Troesch (2004a; 2004b) is a relevant first step in the analysis of real vessels operating in real seaways.

5 Conclusions

From the study presented herein the usefulness of the Lyapunov exponent and short time Lyapunov exponent as analytical tools for studying vessel capsize is investigated. To summarize:

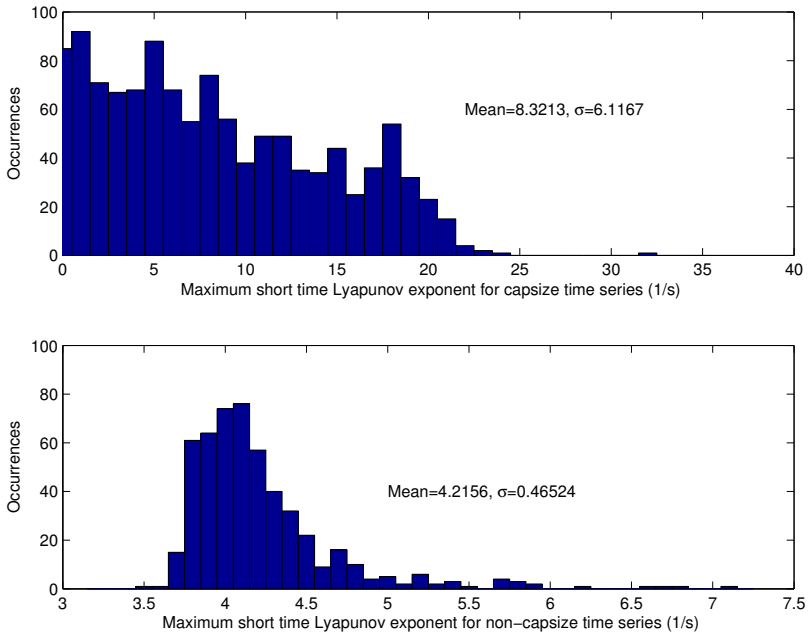

Figure 7: Histograms indicating range of short time Lyapunov exponent values for runs leading to capsize and non-capsize.

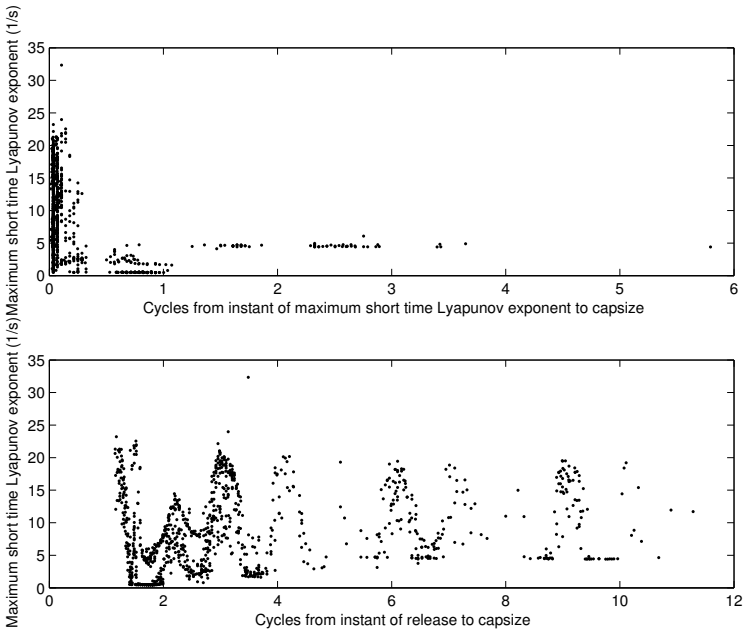

Figure 8: (top) Peak value of largest local Lyapunov exponent as a function of the number of cycles from peak exponent to capsize. (bottom) Peak value of largest local Lyapunov exponent as a function of the number of cycles from release to capsize.

- The Lyapunov exponent is a fundamental system parameter taking on fixed values in the non-capsize region with minimal transitional areas. It can be used to isolate regions of questionable stability to aid in the reduction of test matrices.
- The Lyapunov exponent is shown effective as a validation tool for capsize simulators. Through consistency between the magnitude of a system parameter such as the Lyapunov exponent for large amplitude roll motions measured from an experimental time series and those measured from a numerical simulator, it is possible to demonstrate that the numerical model is capturing the inherent physics of the problem.
- The inherent ineffectiveness of the Lyapunov exponent to yield informative results for the capsize problem is demonstrated. Rather, the importance of calculating a finite time value, such as a short time Lyapunov exponent is discussed.
- From the calculation of the short time Lyapunov exponent further system information is gained which can be used as a predictive tool to indicate lost stability potentially leading to capsize. However, more work must be done to further identify the different types of capsize as characterized by small and large short time Lyapunov exponents.

Acknowledgements

The authors wish to express their gratitude for funding on this project from the Department of Naval Architecture and Marine Engineering at the University of Michigan and the National Defense Science and Engineering Graduate Fellowship program.

References

Arnold, L., Chueshov, I., & Ochs, G. 2003. *Stability and capsizing of ships in random sea-a survey.* Tech. rept. 464. Universität Bremen Institut für Dynamicsche Systeme.

Bay, John S. 1999. *Fundamentals of Linear State Space Systems.* McGraw-Hill.

Benettin, Giancarlo, Galgani, Luigi, Giorgilli, Antonio, & Strelcyn, Jean-Marie. 1980. Lyapunov characteristic exponents for smooth dynamical systems and for Hamiltonian systems; a method for computing all of them. *Meccanica*, 9–20.

Dalzell, J.F. 1978. A Note on the Form of Ship Roll Damping. *Journal of Ship Research*, **22**(3), 178–185.

Eckhardt, Bruno, & Yao, Demin. 1993. Local Lyapunov exponents in chaotic systems. *Physica D*, **65**, 100–108.

Eckmann, J-P, & Ruelle, D. 1985. Ergodic theory of chaos and strange attractors. *Reviews of Modern Physics*, **57**(3), 617–656.

Eckmann, J-P, Kamphorst, S Oliffson, Ruelle, D, & Ciliberto, S. 1986. Liapunov exponents from time series. *Physical Review A*, **34**(6).

Falzarano, Jeffrey M. 1990. *Predicting complicated dynamics leading to vessel capsizing.* Ph.D. thesis, University of Michigan.

Glass, Leon, & Mackey, Michael. 1988. *From Clocks to Chaos.* Princeton, NJ: Princeton University Press.

Haken, H. (ed). 1981. *Chaos and Order in Nature.* New York: Springer-Verlag.

Hegger, Rainer, Kantz, Holger, Schreiber, Thomas, & *et al.* 2000. *TISEAN 2.1, Nonlinear Time Series Analysis.* `http://www.mpipks-dresden.mpg.de/~tisean/TISEAN_2.1/index.html`.

Kantz, Holger. 1994. A robust method to estimate the maximal Lyapunov exponent of a time series. *Physics Letters A*, **185**, 77–87.

Kantz, Holger, & Schreiber, Thomas. 2004. *Nonlinear time series analysis.* Second edn. Cambridge University Press.

Lee, Young-Woo, McCue, Leigh, Obar, Michael, & Troesch, Armin. 2004. Experimental and numerical investigation into the effects of initial conditions on a three degree of freedom capsize model. *Journal of Ship Research.* Tentatively accepted.

Lichtenberg, A.J., & Lieberman, M.A. 1983. *Regular and Stochastic Motion.* New York: Springer-Verlag.

McCue, Leigh S., & Troesch, Armin W. 2003 (September). The effect of coupled heave/heave velocity or sway/sway velocity initial conditions on capsize modelling. *In: 8th International Conference on the Stability of Ships and Ocean Vehicles.*

McCue, Leigh S., & Troesch, Armin W. 2004a (July). Overlay of probability density functions on multi-degree of freedom integrity curves for statistical prediction of critical capsize wave height. Society for Industrial and Applied Mathematics, Annual Meeting, Portland, Oregon.

McCue, Leigh S., & Troesch, Armin W. 2004b. Probabilistic determination of critical wave height for a multi-degree of freedom capsize model. *Ocean Engineering.* Under review.

Murashige, Sunao, & Aihara, Kazuyuki. 1998. Coexistence of periodic roll motion and chaotic one in a forced flooded ship. *International Journal of Bifurcation and Chaos*, **8**(3), 619–626.

Obar, Michael S., Lee, Young-Woo, & Troesch, Armin W. 2001 (September). An experimental investigation into the effects initial conditions and water on deck have on a three degree of freedom capsize model. *In: Fifth International Workshop on the Stability and Operational Safety of Ships.*

Ott, Edward, Sauer, Tim, & Yorke, James (eds). 1994. *Coping with Chaos.* New York: John Wiley and Sons.

Papoulias, Fotis Andrea. 1987. *Dynamic analysis of mooring systems.* Ph.D. thesis, Department of Naval Architecture and Marine Engineering, University of Michigan, Ann Arbor, MI.

Parker, T.S., & Chua, L.O. 1989. *Practical Numerical Algorithms for Chaotic Systems*. New York: Springer-Verlag.

Parlitz, Ulrich. 1992. Identification of true and spurious Lyapunov exponents from time series. *International Journal of Bifurcation and Chaos*, **2**, 155–165. Reprinted in (Ott *et al.*, 1994).

Rosenstein, Michael T., Collins, James J., & De Luca, Carlo J. 1993. A practical method for calculating largest Lyapunov exponents from small data sets. *Physica D*, **65**, 117–134.

Sano, M, & Sawada, Y. 1985. Measurement of Lyapunov Spectrum from a Chaotic Time Series. *Physical Review Letters*, **55**(10).

Schuster, Heinz Georg. 1984. *Deterministic Chaos*. Germany: Physik-Verlag.

Seydel, Rüdiger. 1988. *From Equilibrium to Chaos*. New York: Elsevier Science Publishing.

Thompson, J.M.T., Bishop, S.R., & Leung, L.M. 1987. Fractal basins and chaotic bifurcations prior to escape from a potential well. *Physics Letters A*, **121**(3).

Wolf, A. 1986. *Quantifying Chaos with Lyapunov Exponents*. Chaos. Princeton, NJ: Princeton University Press. Chap. 13.

Wolf, Alan, Swift, Jack, Swinney, Harry, & Vastano, John. 1985. Determining Lyapunov exponents from a time series. *Physica D*, **16**, 285–317.